Wideband Digital Predistortion of Solid-State Radar Amplifiers

ZACHARY DUNN, Student Member, IEEE
MARK YEARY, Fellow, IEEE
CALEB FULTON, Member, IEEE
NATHAN GOODMAN, Senior Member, IEEE
University of Oklahoma
Norman, OK, USA

This paper addresses spectral regrowth caused by wideband signals input into solid-state amplifiers. Unique contributions are a weighted least-squares method for solving predistorter nonlinear model parameters, and a Bayesian method for tracking model parameters in slowly changing systems. Next-generation active phased array radars are the primary application. Past predistortion research has been primarily aimed at narrowband communications, while radar wideband applications have been relatively unexplored. Laboratory measurements confirm our methods.

Manuscript received February 22, 2015; revised December 2, 2015; released for publication July 8, 2016.

DOI. No. 10.1109/TAES.2016.150142.

Refereeing of this contribution was handled by M. Rangaswamy.

Authors' address: Electrical and Computer Engineering, University of Oklahoma, 3190 Monitor Avenue, Norman, Oklahoma 73019, USA. Corresponding author is Z. Dunn, E-mail: (Zachary.T.Dunn-1@ou.edu).

I. INTRODUCTION

Increasingly stringent regulations on bandwidth allocation and management are at odds with growing expectations for future radar system capabilities [1, 2]. In radar systems utilizing coded waveforms with wide instantaneous bandwidths, the fidelity of the transmitted signal is crucial to the ultimate fidelity of the analyzed results of the received signal, as well as the amount of spectral leakage present in the transmitted signal. With this in mind, the transmit chain of a radar system, specifically, the main high-power amplifier (HPA), must be fully characterized so that the final transmitted waveform can be known relative to the desired output waveform. However, physical HPAs exhibit nonlinear behavior over their input power range, which becomes more extreme as the amplifier nears its compression region, where the power-added efficiency of the amplifier is maximized [3–5]. In addition, this nonlinear behavior also varies as a function of input frequency. As a result, HPA modeling can take several forms. The Volterra series is a convenient and compact mathematical model that is capable of modeling systems with both nonlinear behavior and memory effects [6–9]. Nonlinear variations over frequency can be viewed, and thus modeled, as a result of memory effects. With certain assumptions about the system to be modeled, even more compact forms of the Volterra model can be applied. One of these models that is convenient for use with nonlinear and memory-dependent systems with complex input and output data is the memory polynomial (MP) model. Utilizing the MP model, it is possible to accurately model nonlinear behavior and nonlinear variation across an input frequency range.

While knowledge of the actual, distorted output waveform is useful in and of itself, it would be better to use this knowledge to alter the input waveform so that the final distorted output waveform is equal to the desired waveform. The inversion of the HPA model for the purpose of linearizing and equalizing the total system is known generically as predistortion [10]. Digital alteration of an input signal so that the output distorted signal of a system equals the true desired signal is known as digital predistortion (DPD). The model governing DPD for a given radar transmit chain is matched to each individual HPA. Seeing that the DPD must be a nonlinear function of input power and input frequency, DPD can also be modeled with the MP model. DPD allows a given amplifier to output signals that appear to be linearly amplified with minimal distortion, even while the amplifier operates in its compression region, thus maximizing power-added efficiency and significantly reducing spectral regrowth.

Recent advancements in the field of solid-state amplifiers have led to the practical implementation of active array architecture [11–13]. This is in contrast to traditional passive array architecture, where all of the antenna's elements are connected to one power amplifier. Therefore, with each antenna element having its own HPA, maximizing the utility and output of HPAs on an

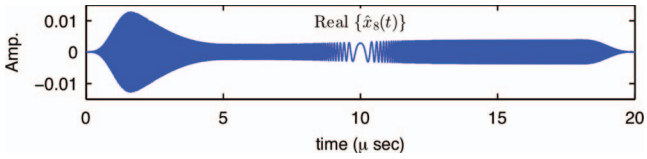

Fig. 1. Example of non-constant-modulus waveform single channel output of wideband beamforming algorithm as shown in [19].

element-by-element basis is crucial to maximizing the capability of the overall wideband radar system. DPD would be ideal for use in this type of architecture, because allowing each amplifier to operate in its compression region without spectral spreading or distortion of the output waveform leads to the maximization of each amplifier's power-added efficiency. This also allows the amplifier to give similar output characteristics of a larger amplifier for waveforms requiring linear amplification. By utilizing smaller amplifiers to their full potential, benefits are quickly recognized in lower cost, lower weight, smaller hardware footprint, easier heat management, smaller and less expensive power supplies, and other associated hardware benefits. When these benefits are multiplied over the number of antenna elements and transmit chains in a given radar system, it can be seen that DPD can have a tremendous effect on the utility of the overall radar system without making drastic and expensive changes to the system's hardware to achieve similar performance.

While DPD has been utilized in communication systems, as in [14–16], it does not have widespread use in radar applications. Whereas adaptive predistortion of unpredictable and constantly changing waveforms is not generally needed in radar systems, DPD in radar applications must apply over a much larger bandwidth at higher power levels in addition to complying with mandated lower sideband suppression than is common in communication systems [17]. This is especially true for wideband radar systems, which is the primary application of this paper. Radar systems typically have a finite number of waveforms to be used during operation, and the waveform to be transmitted is usually known prior to transmission. As a result, adaptive predistortion is not needed at every transmit pulse. Instead, the predistorted version of the input waveforms can be saved into memory to be re-created during operation. The desired waveform is produced at the output of the amplifier, even though this step only requires the same amount of computational power as re-creating the non-predistorted waveform from memory. With this in mind, it can be seen that while conservative implementation of DPD on an active phased array radar requires digital waveform creation, it does not require significant excess computational power. This makes it attractive for modern and emerging architectures in environments where precise spectral usage is required [18], particularly for systems that can utilize non-constant-modulus waveforms with broad instantaneous bandwidth, such as multi-input–multi-output (MIMO) radar systems, low probability of intercept (LPI) radars,

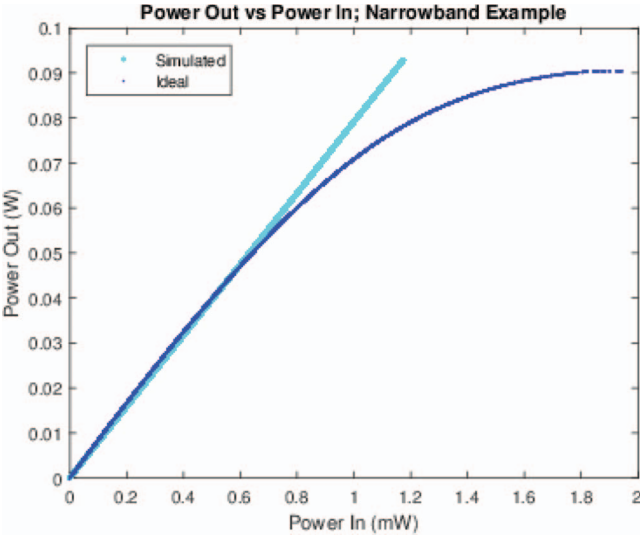

Fig. 2. Example of power out versus power in of well-behaved narrowband and ideal amplified signals.

and synthetic aperture radar (SAR) systems utilizing wideband beamforming. An example of a non-constant-modulus waveform for use in a wideband beamforming algorithm proposed by [19] is shown in Fig. 1.

II. TECHNICAL APPROACH TO MODELING AMPLIFIER AND PREDISTORTER

A. Conceptual Approach to DPD

As was previously stated, predistortion is effectively the inversion of a nonlinear HPA model for the purpose of linearizing the output power versus input power relation for the total system. To get a better understanding of what predistortion is actually doing, visual examples will be helpful. Output power versus input power graphs of simulated well-behaved narrowband and measured wideband amplifier data with overlaid ideal outputs are shown in Fig. 2 and Fig. 3, respectively.

At its core, predistortion is essentially remapping a given input signal to a different input signal so that when altered by the HPA's nonlinear distortion, the desired ideal output signal is the result. This ideal output signal has a linear output power versus input power relation with a gain that matches the gain of the linear region of the measured amplifier, as well as a uniformly flat group delay response. Consider the simulated narrowband (i.e., single frequency) output power versus input power graph as shown in Fig. 2. Predistortion effectively takes the ideal output power versus input power relationship and carefully and intentionally rescales the input power so that the new output power versus input power relationship matches the measured nonlinear output power versus input power relationship of the amplifier. This process is relatively simple for the narrowband case: For each ideal output power level, the same measured output power level corresponds with only one measured input power level. The nonlinear equation that determines the particular

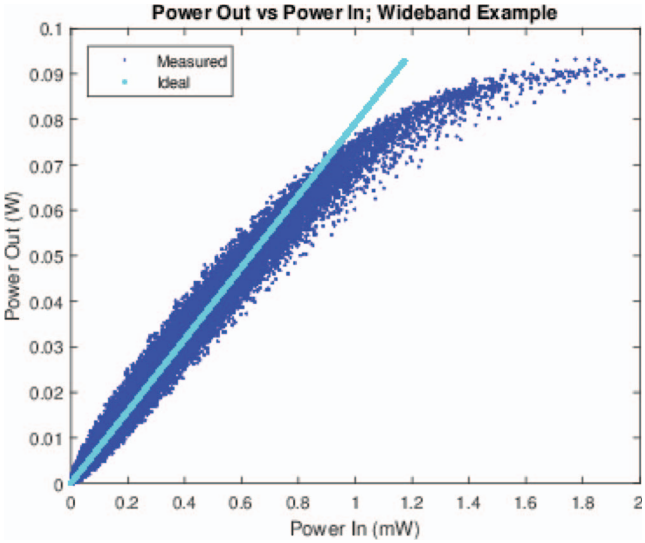

Fig. 3. Example of power out versus power in of measured wideband and ideal amplified signals.

horizontal stretch for a given input power is the predistortion model. Note that the maximum output power of the ideal signal is equal to the maximum output power of the measured signal. This means that the ideal input signal to be predistorted must have an upper power limit corresponding with the power that gives the maximum output power of the measured signal when the gain of the ideal output power versus input power relation is applied.

However, determining the predistortion model for a given amplifier is more complicated than it first appears due to the possibility of variation in the nonlinear behavior of the HPA over the input frequency. The effect of this frequency dependence is readily apparent in the measured wideband case (40 MHz bandwidth), and can be seen in Fig. 3 in the vertical width of the measured sample range for a given input power. The overall shape of the output power versus input power response samples can be thought of as the overlap of samples from numerous power sweeps at constant frequencies spanning the calibration data passband (this is not the case, but it is helpful to think of it in this way for this example). Again, predistortion effectively takes the ideal input signal and rescales it so that the output power versus input power relationship matches the measured nonlinear output power versus input power relationship of the amplifier. However, due to the wideband nature of the input signal and the frequency dependence of the amplifier, there is a measured input power level range that corresponds with any desired ideal output power level. The input power level range for a single output power is composed of a single sample from each of the power sweeps at different frequencies. In order to map the ideal input signal to the correct measured input signal, the "instantaneous" frequency of the ideal input signal must be known. If frequency-based effects were ignored, the vertical width of the predistorted amplified signal would be largely unchanged from that of the measured samples. Note that in the wideband case, the maximum output power of the ideal signal is equal to the maximum vertical lower bound of the measured signal, which corresponds with the "worst-case" maximum power for all frequencies present in the signal. This ensures that the ideal output signal is possible to produce given the frequency effects present in the system. Furthermore, due to the fact that, for a given ideal input signal sample at a given frequency, there is only one correct measured input signal to which that point can be mapped, it is implied that the measured signal data from which the specific predistortion relation and model were derived must have an output power versus input power relation that is monotonically increasing.

It was previously stated that nonlinear variations over frequency can be viewed, and thus modeled, as a result of memory effects. In the equations used to model both the nonlinear distortion of the amplifier as well as the equations used to model the nonlinear distortion of the predistorter, memory terms are simply terms of the causal polynomial that are functions of one or more delayed input signal samples. The presence of memory terms in a model's polynomial establishes effects within the output signal that are dependent upon the relation between input samples at fixed time interval differences (i.e., intervals of the sampling rate). The relation between input samples at fixed time interval differences can be interpreted as being frequency related, and thus the introduction of memory terms allows frequency-based effects to be reliably modeled.

B. Volterra Series and MP Model

The Volterra series is useful for modeling systems with both nonlinearities and memory effects, and it is ideal for modeling the output of HPAs and their associated predistortion models. The general form of the discrete Volterra series is given by

$$y_V(n) = \sum_{k=1}^{K} y_k(n) \tag{1}$$

where

$$y_k(n) = \sum_{m_1}^{M-1} \cdots \sum_{m_k}^{M-1} h_k(m_1, \ldots, m_k) \prod_{l=1}^{k} x(n - m_l) \tag{2}$$

where $y_V(n)$ is the output sample, $x(n)$ is the input sample, K is the order of nonlinearity of the system, M is the order of memory of the system, and $h_k(m_1, \ldots, m_k)$ is a coefficient with set values as a function of k and m_1 through m_k. The general form of the Volterra series is capable of modeling nonlinear systems with memory effects due to the extensive number of coefficients paired with every combination of input sample and delayed input sample combinations within the bounds of the specified nonlinear order and memory order of the model. The general form of the Volterra series is therefore able to model systems with both large nonlinearities and significant memory effects, and higher precision and more

accurate modeling can be provided by simply raising the nonlinear and memory orders of the model. However, the number of coefficients, and thus computational complexity in calculating the coefficients, increases at a substantial rate as either the nonlinear order or the memory order of the model is increased. With this in mind, many simplifications of the full Volterra model, with fewer coefficients and reduced complexity of calculation, have been devised and studied [20–22]. One of the simplified Volterra-based models that has had previous success modeling physical amplifiers at complex baseband is the memory polynomial model [20, 23–26]. The MP model is given by

$$y(n) = \sum_{k=0}^{K-1} \sum_{m=0}^{M-1} h_{km} x(n-m)|x(n-m)|^k \tag{3}$$

where $y(n)$ is the output sample, $x(n)$ is the input sample, K is the order of nonlinearity of the system, M is the order of memory of the system, and h_{km} is a coefficient with set values as a function of k and m.

Due to the MP model being linear with respect to the coefficients, it can be represented efficiently in matrix form. This applies both to the amplifier model and its associated predistortion function. These matrix representations readily allow the coefficients to be determined for either case by using a set of measured input and output data, as detailed herein. Because the MP model is fundamentally composed of a summation of coefficients that are each paired with delayed powers of the input waveform, it can be represented efficiently in matrix form as $\mathbf{y} = \mathbf{X}\boldsymbol{\theta}_{MP}$. This matrix representation can be expanded to be shown as

$$\mathbf{y} = \begin{bmatrix} y(M) \\ \vdots \\ y(N) \end{bmatrix} = \mathbf{X} \begin{bmatrix} h_{00} \\ \vdots \\ h_{0m} \\ \vdots \\ h_{k0} \\ \vdots \\ h_{km} \end{bmatrix} \tag{4}$$

and $\boldsymbol{\theta}_{MP}$ is a $[B \times 1]$ column vector containing all the coefficients h_{km}. It should be noted that N is equal to the length of the input vector $\mathbf{x}$, and B is equal to the number of coefficients for a given nonlinear order and memory order of the MP model, while $A = N - (M - 1)$, which ensures that any generated output in $\mathbf{y}$ was calculated with populated values for the necessary delayed input terms. The delay matrix is composed of the varying combinations of input terms that are both delayed and not delayed associated with the B coefficients for each of the A output samples to be created. This means that the delay matrix can be created given only the input sample array and the order of nonlinearity and memory order of the MP model to be used. The $[B \times 1]$ model coefficient column vector $\boldsymbol{\theta}_{MP}$ contains the unknown coefficients h_{km}, which collectively capture HPA behavior over the power and frequency ranges of interest. High-fidelity measurements of the amplifier output, excited by a strategically chosen and well-known input signal, are required to estimate the coefficients in $\boldsymbol{\theta}_{MP}$. This pair of data is known as the calibration data set, and it should be chosen so that the input signal excites across the entire bandwidth and power ranges over which the amplifier is to be modeled [27]. A good way to capture as much of the nonlinearity effects and memory effects as possible is to generate a random signal spanning the desired power range before filtering the signal to the desired bandwidth. This random signal approach creates many combinations of input power and frequencies that help to excite the amplifier in as many different states as possible, leading to more behavior of the amplifier being recorded. As a result, when using the frequency-filtered random signal approach to generating calibration data, the longer the signal is in time, the better the system will be characterized. With this in mind, it is useful to choose calibration data containing a large number of sample points, although the length of the calibration input signal is practically limited by the computational power needed to analyze the calibration data when calculating the MP model coefficients. Once a suitable calibration data set is acquired for an HPA, and the order of nonlinearity and order of memory for the MP model are chosen, the coefficient column vector $\boldsymbol{\theta}_{MP}$ can be calculated. This is accomplished by minimizing the squared error with respect to the coefficient vector, where

$$\mathbf{X} = \begin{bmatrix} x(M) & \cdots & x(1) & \cdots & x(M)|x(M)|^k & \cdots & x(1)|x(1)|^k \\ \vdots & & \vdots & & \vdots & & \vdots \\ x(N) & \cdots & x(N-M+1) & \cdots & x(N-M+1)|x(N-M+1)^k & \cdots & x(N-M+1)|x(N-M+1)|^k \end{bmatrix} \tag{5}$$

where the $[A \times B]$ matrix $\mathbf{X}$ is called the delay matrix and is shown partially expanded in (5), $\mathbf{y}$ is an $[A \times 1]$ column vector containing the calculated outputs of the MP model, the error is defined as the difference between the calculated calibration output samples and the measured calibration output samples. This least-squares

minimization problem is shown as

$$\min_{\boldsymbol{\theta}_{MP}} \|\mathbf{y}_{cal} - \mathbf{X}_{cal}\boldsymbol{\theta}_{MP}\|^2 = \min_{\boldsymbol{\theta}_{MP}} \left[\mathbf{y}_{cal}^{\mathrm{H}}\mathbf{y}_{cal} - \mathbf{y}_{cal}^{\mathrm{H}}\mathbf{X}_{cal}\boldsymbol{\theta}_{MP} - \boldsymbol{\theta}_{MP}^{\mathrm{H}}\mathbf{X}_{cal}^{\mathrm{H}}\mathbf{y}_{cal} + \boldsymbol{\theta}_{MP}^{\mathrm{H}}\mathbf{X}_{cal}^{\mathrm{H}}\mathbf{X}_{cal}\boldsymbol{\theta}_{MP}\right] \quad (6)$$

where $\mathbf{y}_{cal}$ is the measured output signal column vector of the calibration data, $\mathbf{X}_{cal}$ is the delay matrix formed by the calibration data input signal $\mathbf{x}_{cal}$, and $[\cdot]^{\mathrm{H}}$ is the complex conjugate transpose operator. Setting the derivative of (6) equal to zero and solving for $\boldsymbol{\theta}_{MP}$ yield the least-squares solution, shown as

$$\boldsymbol{\theta}_{MP} = (\mathbf{X}_{cal}^{\mathrm{H}}\mathbf{X}_{cal})^{-1}\mathbf{X}_{cal}^{\mathrm{H}}\mathbf{y}_{cal} \quad (7)$$

This well-known solution is referred to as the Moore-Penrose pseudoinverse [28, 29]. Once the coefficients of the MP model have been found, if adequate values for the order of nonlinearity and order of memory were selected, and the range of input power levels and range of frequencies present in an input signal array fall within those represented by the calibration data input signal, then the realistic output of the HPA can be simulated. It should be noted that if $\boldsymbol{\theta}_{MP}$ remains unchanged throughout simulations following calibration, the method used to assemble the calibration data delay matrix given the calibration data's input signal should be used to assemble all future delay matrices given a desired input signal. This will ensure that the MP model coefficients for the given model are always correctly paired with their associated delayed and nondelayed input signal combinations.

It is desired not only to create a realistic model of the HPA, but also a model of an associated predistortion function that can be used in conjunction with the HPA to create an overall linearly behaving system. More specifically, when the DPD is paired with the HPA, the desired signal input into the DPD will be reproduced at the output of the HPA multiplied only by the gain corresponding with the linear region of the HPA. Therefore, the model of the DPD is basically an inverse of the model of the HPA. Due to the HPA exhibiting both nonlinearities and memory effects, the DPD will need to account for both nonlinearities and memory effects. However, because the HPA is successfully modeled by the MP model, this also means that the HPA's associated DPD can also be successfully modeled using the MP model, given by $\mathbf{y} = \mathbf{X}\boldsymbol{\theta}_{PD}$, where $\mathbf{y}$ is the DPD output signal column vector, $\mathbf{X}$ is the delay matrix formed by the DPD input signal, and $\boldsymbol{\theta}_{PD}$ is a column vector containing all the MP model coefficients of the DPD. The order of nonlinearity and order of memory for the DPD may differ from the order of nonlinearity and order of memory used in the model of the HPA. The coefficients of the MP model for the DPD can be calculated in a similar way as the method used to find $\boldsymbol{\theta}_{MP}$ using the Moore-Penrose pseudoinverse and a set of calibration data. In order to calculate the values of the coefficient column vector $\boldsymbol{\theta}_{PD}$ so that the DPD will be a match with the given amplifier, the same set of calibration data is used, but it is scaled and used in reverse order. The calibration data input signal column vector $\mathbf{x}_{cal}$ remains unscaled, but the calibration data output signal $\mathbf{y}_{cal}$ is rescaled so that, when multiplied by the HPA's linear region gain, the maximum magnitude equals the maximum magnitude of the measured calibration data input signal. The Moore-Penrose pseudoinverse is executed, and the coefficient column vector $\boldsymbol{\theta}_{PD}$ is found by

$$\boldsymbol{\theta}_{PD} = (\mathbf{Y}_{cal}^{\mathrm{H}}\mathbf{Y}_{cal})^{-1}\mathbf{Y}_{cal}^{\mathrm{H}}\mathbf{x}_{cal} \quad (8)$$

where $\mathbf{Y}_{cal}$ is the delay matrix formed by the rescaled calibration data output signal $\mathbf{y}_{cal}$. Once the coefficients of the MP model for the DPD have been found, if adequate order of nonlinearity and order of memory were selected, and the range of input power levels and range of frequencies present in the input signal array fall within those allowed by the calibration data, then the necessary predistorted signal can be simulated. It should be noted that the allowed range of frequencies for the input signal is equal to the range of frequencies represented by the calibration data. However, the allowed range of amplitudes is limited by the maximum magnitude of the rescaled calibration data output signal $\mathbf{y}_{cal}$ that was used to solve for $\boldsymbol{\theta}_{PD}$, which was previously decided to be the magnitude that, when multiplied by the HPA's linear region gain, equals the maximum magnitude of the calibration data input signal. It should also be noted that in the way the DPD coefficient column vector $\boldsymbol{\theta}_{PD}$ was found, these coefficients are actually the necessary coefficients for a MP model postinverse filter. However, due to the inherent quality of the Volterra series in which the pth order postinverse of a Volterra series is equal to the pth order pre-inverse of a Volterra series, the coefficients found for the postinverse model can be used as the coefficients of a pre-inverse model instead [30]. Therefore, by using two different realizations of the MP model simplification of the Volterra series and a single set of calibration data, it is possible to not only successfully model the output of a HPA given an input signal, but it is also possible to find the necessary DPD model that, when used in series with the HPA, will make the overall transmit chain behave as a linear system.

In summary, the DPD process requires a measured set of calibration data with a known linear region, predefined orders of nonlinearity and memory for both the amplifier and DPD models, and a desired input signal. The DPD process results in the creation of the amplifier and DPD model coefficients, predistorted input waveform, simulated predistorted amplified output waveform, and the measured predistorted amplified output waveform. This process is visually summarized in Fig. 4.

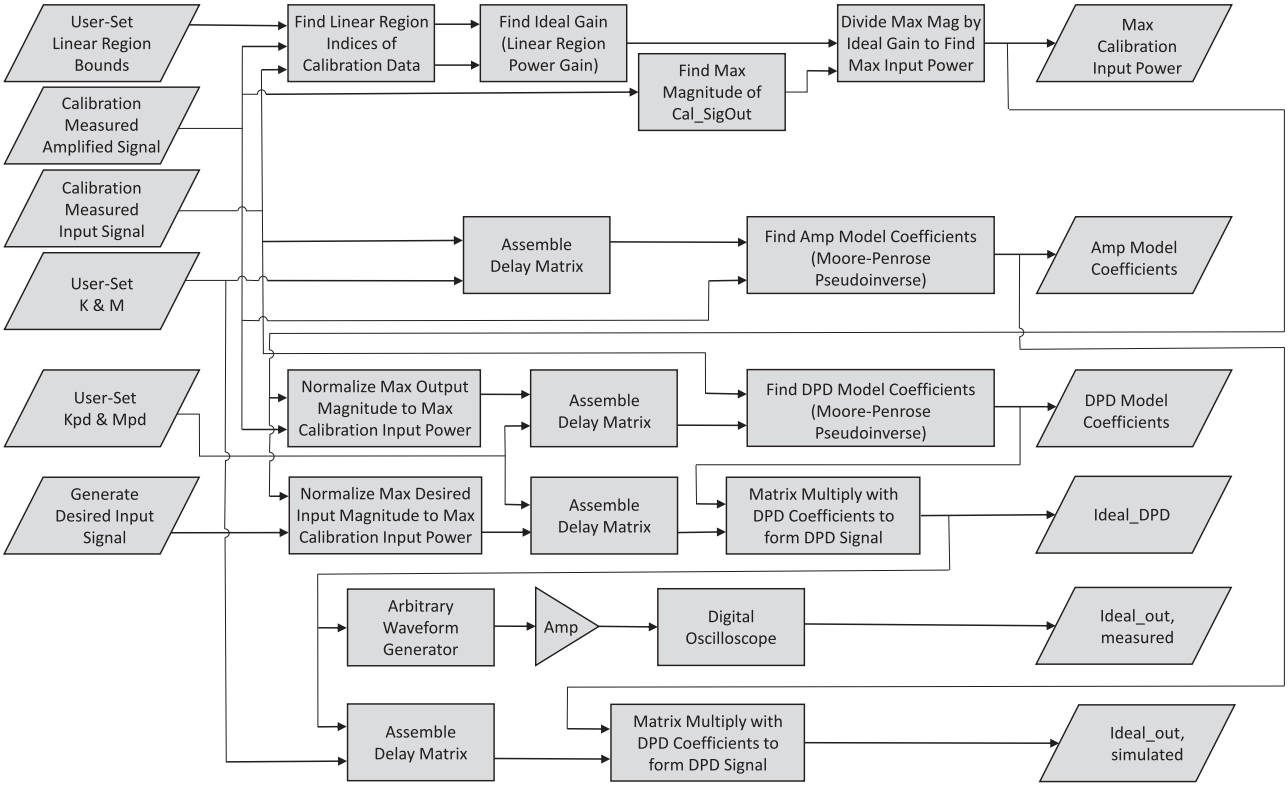

Fig. 4. Flow chart summary of DPD process.

C. Weighting for Numerical Stability of Least-Squares Model Solution

When the specified order of nonlinearity of the HPA or DPD model is large, numerical instabilities can begin to arise when solving for the model coefficients by executing the Moore-Penrose pseudoinverse. While other approaches have been proposed to make the pseudoinverse more numerically stable for large-order polynomials by modifying the MP model itself [31], it was decided in this context to normalize the delay matrices of both the HPA model and the DPD model by dividing each individual term of the delay matrix by the maximum magnitude of the calibration input signal for that particular delay matrix to the power corresponding with the order of nonlinearity of the particular term in the delay matrix. This can be represented by introducing a weighting matrix $\mathbf{W}$, substituting $\mathbf{X}_{\mathrm{w}}$ for $\mathbf{X}$ in (4) and (7), where

$$\mathbf{X}_{\mathrm{w}} = \mathbf{X}\mathbf{W} \tag{9}$$

Similarly for (8), $\mathbf{Y}_{\mathrm{cal,w}}$ is substituted for $\mathbf{Y}_{\mathrm{cal}}$, where $\mathbf{Y}_{\mathrm{cal,w}} = \mathbf{Y}_{\mathrm{cal}}\mathbf{W}$. The elements $\mathbf{W}_{i,j}$ of the square weighting matrix $\mathbf{W}$ of dimensions $[B \times B]$ are represented by

$$\mathbf{W}_{i,j} = \begin{cases} \dfrac{1}{(x_{cal,max})^{K_j}} & \text{for } i = j \\ 0 & \text{for } i \neq j \end{cases} \tag{10}$$

where $x_{\mathrm{cal,max}}$ is the maximum instantaneous magnitude present in the calibration data signal used to assemble the delay matrix, and K_j is the order of nonlinearity associated with the jth coefficient term in the selected MP model.

This results in each individual term of the delay matrix being scaled so that, for a given input time signal, the range of typical values spanned by the varying nonlinear terms is reduced by several orders of magnitude. As a result, when this normalized delay matrix is used in the Moore-Penrose pseudoinverse for finding the coefficients of the model, the least-squares solution for the coefficients is produced with a much more balanced importance being placed on each term as the order of nonlinearity associated with that term changes. This normalization process effectively creates a weighted least-squares approach, with more accurate and numerically stable HPA simulation and DPD results than previous approaches, such as [9].

The stability of the Moore-Penrose pseudoinverse can be inspected quantitatively by the matrix condition number, more specifically, the condition number of the delay matrix. The condition number is a common linear algebra tool for examining the sensitivity of a solution for a system of linear equations to error [32–34]. In the case of the amplifier MP model, the condition number can be thought of as the maximum ratio of the relative error in the coefficients divided by the relative error in the measured output signal. A matrix is said to be well conditioned if the condition number is close to 1, and it is said to be ill conditioned if the condition number is extremely large. Using a set of calibration data measured through a Specwave QBH-7-4012 amplifier, the condition number of

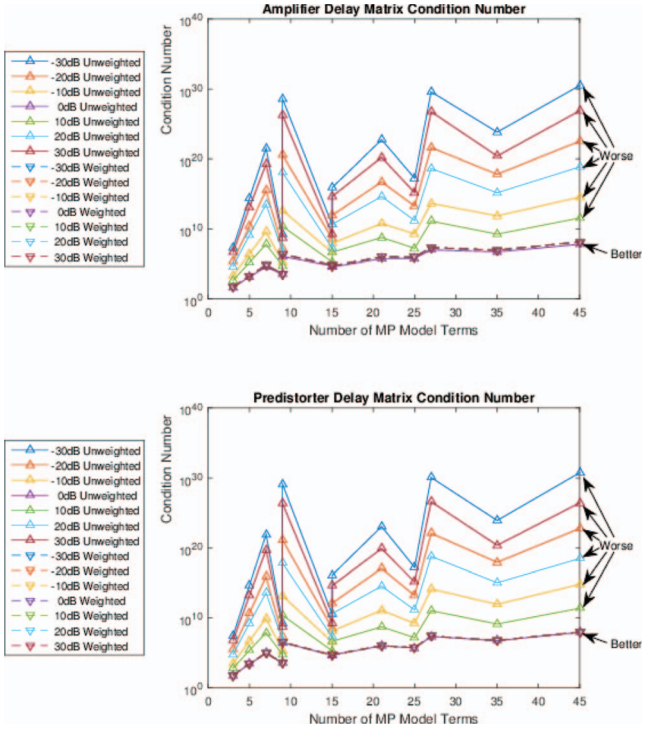

Fig. 5. Delay matrix condition number for amplifier and DPD MP models as a function of number of model terms. Note that the condition numbers resulting from the weighted approach are more stable regardless of scaling.

the delay matrix was calculated using both the unweighted and weighted least-squares approaches. In order to examine various ranges of possible calibration data input values and their effect on the calculated condition number, the input and output calibration data were rescaled at decade increments from -30 dB to $+30$ dB. At each level of scaled calibration data, the delay matrix condition number was calculated for various model parameters, specifically, for all permutations of models with order of nonlinearity equal to three, five, seven, or nine and with order of memory equal to one, three, or five. These calculations were made for both the amplifier and DPD delay matrices. The comparison between the weighted and unweighted approaches can be seen in Fig. 5. It is observed that for both the amplifier and DPD cases, the weighted least-squares–based approach results in relatively low condition numbers that remain very stable as the magnitude of the calibration data is altered, whereas the unweighted least-squares–based approach can have largely varying condition numbers that are nearly always orders of magnitude larger than those computed with the weighted approach.

In general, for both the weighted and unweighted approaches, the matrix condition number increases as the number of coefficients in the MP model increases. Our successfully measured results utilizing the weighted least-squares approach, presented later in section III, confirm our theoretical formulations.

D. Bayesian Analysis for Model Parameter Refinement and Slowly Changing Systems

While the Moore-Penrose pseudoinverse method of finding the least-squares solution was used in the previous sections for finding the coefficient values for both the amplifier model and the predistortion function, there are other methods available for calculating nonlinear model parameters that offer benefits [35, 36]. One of these methods is Bayesian analysis utilizing Gibbs sampling, which is a form of the Markov chain Monte-Carlo (MCMC) algorithm that approximates the multivariate probability distribution of the model parameters. Whereas the Moore-Penrose least-squares solution uses all available measured calibration data in each execution to find parameter values, Bayesian analysis uses only the latest acquired calibration set of data in conjunction with a multivariate probability containing all prior knowledge of the system, known as a prior, to construct probabilities of the model parameters. Once the posterior conditional probabilities of the parameters are found, the mean of each is calculated to give point estimates for the parameters. Under the belief that the best model parameters are chosen when the greatest amount of calibration data is utilized, the Bayesian approach offers a significant computational advantage if the system continually acquires calibration data throughout operation. In addition, the Bayesian approach can result in parameters that are capable of accurately tracking the best underlying model in the presence of slowly varying system conditions [37]. The inherent ability of the Bayesian approach to correctly alter amplified nonlinear model parameters as the system changes is in contrast to the previous least-squares only approach, such as [38, 39], which, in a changing system environment with continuous training data acquisition, can only result in a parameter set that is the least-squares solution to the system state that is essentially the average of all measured system states, rather than the current system state.

The model used for Bayesian analysis is based on the unweighted MP model shown in (3), but due to the Gibbs sampling program operating only on real numbers, the original complex MP model is converted into two real equations representing the real and imaginary components individually. These equations are shown as

$$\hat{y}_r[n] = \sum_{k=0}^{K-1}\sum_{m=0}^{M-1}\Big(\big(h_{km,r}x_{cal,r}[n-m] - h_{km,i}x_{cal,i}[n-m]\big) \times \sqrt{x_{cal,r}^2[n-m] + x_{cal,i}^2[n-m]}^{\,k}\Big) \tag{11}$$

and

$$\hat{y}_i[n] = \sum_{k=0}^{K-1}\sum_{m=0}^{M-1}\Big(\big(h_{km,i}x_{cal,r}[n-m] + h_{km,r}x_{cal,i}[n-m]\big) \times \sqrt{x_{cal,r}^2[n-m] + x_{cal,i}^2[n-m]}^{\,k}\Big) \tag{12}$$

where $\hat{y}[n]$ is the calculated MP model values with $\hat{y}[n] = \hat{y}_r[n] + \mathrm{j}\,\hat{y}_i[n]$, the measured input calibration signal $x_{cal}[n] = x_{cal,r}[n] + \mathrm{j}\,x_{cal,i}[n]$, and the complex MP model coefficients $h_{km} = h_{km,r} + jh_{km,i}$. The measured output calibration signal is defined to be the result of a compound normal distribution, shown as

$$y_{cal,r}[n] \sim \mathrm{N}(\mu = \hat{y}_r[n], \tau = \tau_{y,r}) \tag{13}$$

and

$$y_{cal,i}[n] \sim \mathrm{N}(\mu = \hat{y}_i[n], \tau = \tau_{y,i}) \tag{14}$$

where the measured output calibration signal $y_{cal}[n] = y_{cal,r}[n] + \mathrm{j}\,y_{cal,i}[n]$, the distribution's mean is the MP model value $\hat{y}[n]$ calculated using the measured input calibration signal, and the distribution's precision τ is a model variable itself. Once the multivariate posterior probability distribution of the model's variables has been calculated, the point estimate of each conditional probability is calculated, giving the MP model coefficient estimates as well as the precision of the compound normal distribution approximating the model about the measured data. The distribution approximating the model output is compound normally distributed due to the precision itself being an unknown distribution.

A single set of calibration data with a bandwidth of 40 MHz was used, implying the underlying assumption of a completely steady-state system. Additionally, all parameters for the Bayesian algorithm were initialized with uninformative priors, and it was found that the weighted least-squares approach generated model parameters that had slightly better results than those generated by the Bayesian-generated coefficients. This resulted in amplifier models with results closer to measured values and DPD models that resulted in less spectral spreading. However, when amplifier characteristics changed due to changing unmodeled system parameters, such as the temperature of the amplifier, the Bayesian-generated coefficients gave much more satisfactory results because the system was able to track with the changes while still incorporating and adding to historical data about the amplifier. These results are seen in Fig. 6, which shows the $K = 9$, $M = 5$ amplifier models generated by both the least-squares and Bayesian analysis approaches as the amplifier undergoes a temperature shift, with each subsequent row representing a progression in amplifier state. The predicted output power versus input power for both approaches is plotted in addition to the current measured amplifier output power versus input power in the left column of Fig. 6. The difference between both modeled amplifier output powers and the current measured amplifier output power is plotted in the right column of Fig. 6. It can be easily seen that the difference between the measured and modeled results is less for the least-squares approach when the system is stable, but it is less for the Bayesian-generated approach as the system changes. The calibration data set was formed by concatenating four calibration data sets that were each recorded during the warm-up period of a Specwave QBH-7-4012 amplifier, with the four 40 MHz bandwidth measurements taken at delays of 0, 1, 5, and 10 min after amplifier activation, respectively.

III. PREDISTORTION OF DIGITALLY CODED WAVEFORMS

Simulations and tests were conducted on a representative non-constant-modulus waveform that spanned the power and bandwidth of a possible wideband radar waveform, as well as a constant-modulus–constrained coded waveform typical of a wideband radar. The P4 coded waveform was chosen to represent a typical wideband constant-modulus radar waveform, because it is a polyphase code with broad instantaneous bandwidth. Although polyphase codes have been known for some time, P4 codes have gained in popularity over the last several years because they are efficient to digitally synthesize and have unique applications in modern radars, for example [40–42] and others. New classes of good polyphase code sets can be generated using pieces of P4 polyphase codes, and these code sets are suited for many applications, including orthogonal netted radar systems (ONRS) and MIMO radars [41]. Under the cross-correlation elimination (CCE) condition, many monostatic radar waveforms can be directly used in the MIMO radar system, such as P4 codes [42]. As noted by Lewis and Kretschmer [43], the P4 polyphase pulse compression code is very Doppler tolerant, can provide large pulse compression ratios, and is tolerant of precompression bandwidth limitations. Therefore, the P4 code and its results represent any typical wideband constant-modulus radar waveform with wide instantaneous bandwidth, including, but not limited to, Frank, P1, P2, P3, biphase, or polyphase modulated waveforms.

The non-constant-modulus waveform chosen to represent any possible wideband radar waveform within the system's filtered bandwidth range consisted of a randomly generated complex baseband signal filtered to the bandwidth at which the system was to be characterized. Although the available test setup hardware limited the calibration waveform to a relative bandwidth that was not overly large, the chosen bandwidth was sufficient to capture wideband effects of the amplifier. This is demonstrated by the large vertical width of the output power for a single input power as seen in section IIID. Therefore, this randomly generated code and its results represent any radar waveform with wide instantaneous bandwidth and non-constant modulus. Waveforms with these attributes could be encountered in more specialized and advanced radar system roles, such as MIMO systems, LPI radars, and SAR wideband beamforming applications. Due to the assumption of a steady-state system, these waveforms were predistorted utilizing the weighted least-squares–based method described in section III, and the simulated and measured results were compared to the respective non-predistorted cases. This was done to test

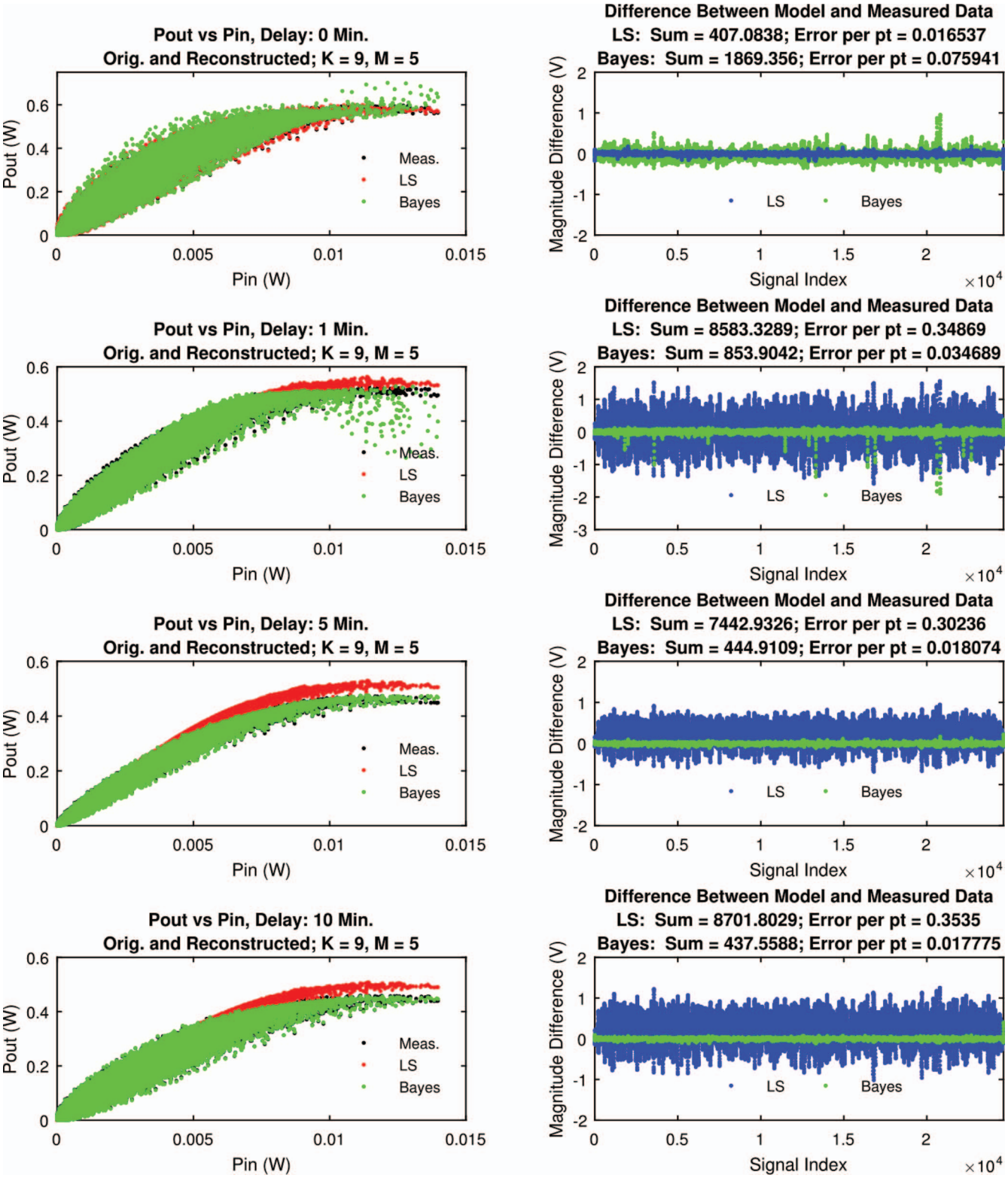

Fig. 6. Measured amplifier data versus least-squares and Bayesian model results.

the ability of the DPD to match the final distorted output waveform to the desired output waveform in a steady-state system, and to quantify the effect on spectral spreading behavior while the amplifier operated in its compression region. Through trial and error, it was found that $K = 9$ and $M = 5$ for the MP DPD orders provided optimal performance for the given test data sets.

For both the constant-modulus and non-constant-modulus waveforms tests, it was expected that the simulated predistorted results would have slightly better

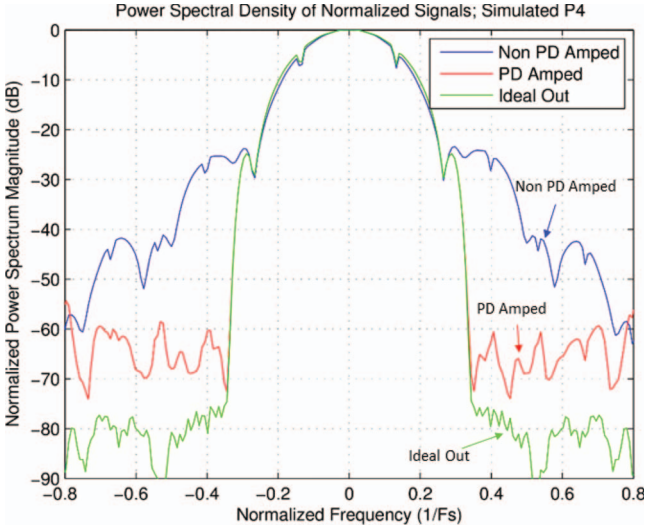

Fig. 7. Power spectral density of simulated predistorted and non-predistorted P4-coded waveforms after HPA distortion.

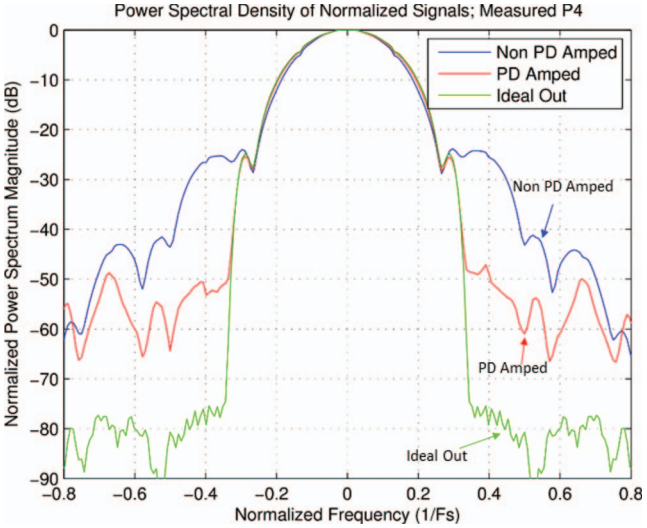

Fig. 8. Power spectral density of measured predistorted and non-predistorted P4-coded waveforms after HPA distortion.

suppressed spectral spreading than their physically measured counterparts. This is due to the fact that the predistorted and non-predistorted signals in a physically measured test are being applied to a real system with nonlinear characteristics, rather than a known model approximating a system with nonlinear characteristics. Therefore, when a simulation is executed, the exact nonlinear behavior of the simulated amplifier is already known, whereas the measured test will have some element of noise or unmodeled and unaccounted for effect present simply due to the fact that a physical amplifier's nonlinear behavior cannot be perfectly known. This expectation was confirmed, and for both the constant-modulus and non-constant-modulus waveform tests, the magnitude of the spectral spreading was slightly lower for the simulated case than for the respective physically measured case.

A. P4 Waveform Simulation

A simulated system was analyzed using calibration data measured through a Specwave QBH-7-4012 amplifier and a constant-modulus, 20 MHz, P4-coded waveform filtered to a bandwidth of 40 MHz. A 40 MHz filter was chosen in order to capture the null-to-null waveform information. The waveforms had a pulse width of 84 μs and a maximum input voltage equal to the maximum allowed magnitude as specified by analysis of the calibration data. Using an HPA model with $K = 9$ and $M = 5$, it was seen that the digitally predistorted signal was nearly an exact match to the desired output signal. The non-predistorted signal, which was equal to the DPD input signal and scaled so that its maximum magnitude corresponded with the predistorted signal's maximum magnitude, experienced nonlinear distortion and compression across the span of the waveform. The spectral spreading of the non-predistorted output signal was much larger than that of the predistorted signal after being distorted by the HPA. This is seen in Fig. 7. With these results in mind, it can be seen that using the DPD model on the input waveform leads to a much more desirable simulated result, closely matching the ideal output signal, and with a much smaller degree of spectral spreading than would be present without DPD.

B. P4 Waveform Test in Hardware

The same P4-coded waveform used in simulation was generated with a center frequency of 1.2 GHz and amplified through a Specwave QBH-7-4012 amplifier and tested both with and without DPD. Using a pulse width of 84 μs and a maximum input voltage equal to the maximum allowed magnitude as specified by analysis of the calibration data, Fig. 8 shows that the digitally predistorted signal had much lower measured spectral spreading than the non-predistorted signal. This demonstrates DPD's potential impact on modern wideband radar signals, where high-gain systems utilizing waveforms with broad instantaneous frequency can be predistorted to have much improved spectral characteristics.

C. Non-Constant-Modulus Waveform Simulation

A simulated system was analyzed using calibration data measured through a Specwave QBH-7-4012 amplifier and a representative non-constant-modulus test signal composed of a randomly generated complex baseband signal filtered to a bandwidth of 40 MHz, a pulse width of 25 μs, and a maximum input voltage equal to the maximum allowed magnitude as specified by analysis of the calibration data. Using an HPA model with $K = 9$ and $M = 5$, it was seen that the digitally predistorted signal was nearly an exact match to the desired output signal. However, the non-predistorted signal, which was equal to the DPD input signal scaled so that its maximum magnitude corresponded with the predistorted signal's maximum magnitude, experienced nonlinear distortion and compression across the span of the waveform. The

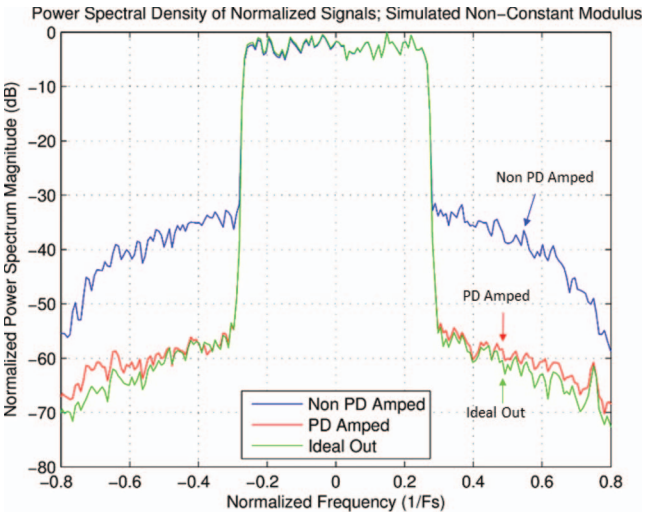

Fig. 9. Power spectral density of simulated predistorted and non-predistorted signals after HPA distortion.

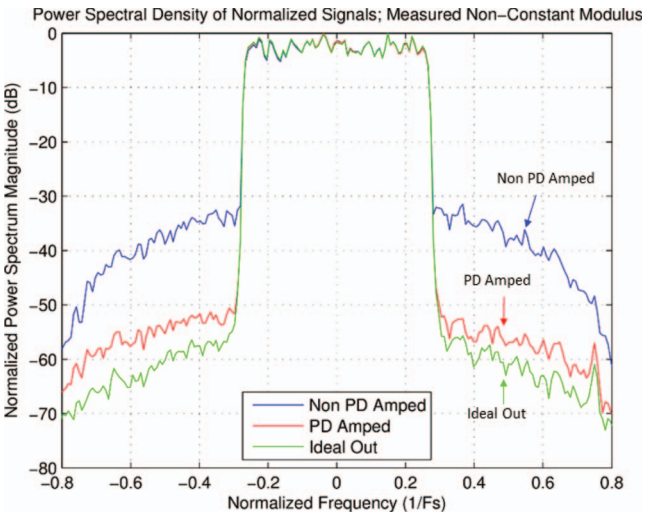

Fig. 10. Power spectral density of measured predistorted and non-predistorted signals after HPA distortion.

spectral spreading of the non-predistorted output signal was also much larger than that of the predistorted signal after being distorted by the HPA. This is seen in Fig. 9. With these results in mind, it can be seen once again that using the DPD model on the input waveform leads to a much more desirable simulated result, closely matching the ideal output signal, and with a much smaller degree of spectral spreading than would be present without DPD.

D. Non-Constant-Modulus Waveform Test in Hardware

The same non-constant-modulus representative test signal used in simulation was generated with a center frequency of 1.2 GHz and amplified through a Specwave QBH-7-4012 amplifier and tested both with and without DPD. Using a pulse width of 25 μs and a maximum input voltage equal to the maximum allowed magnitude as specified by analysis of the calibration data, Fig. 10 shows that the digitally predistorted signal had much lower measured spectral spreading than the non-predistorted signal.

Fig. 11 demonstrates that the measured predistorted signal closely matches the ideal linear gain across the output power range. The large vertical width of the measured non-predistorted signal for a given input power is due to the wideband nature of the waveform in conjunction with the frequency dependency of the amplifier. The vertical narrowing of the predistorted signal is due to frequency dependency correction, demonstrating that the order of memory chosen for the model is sufficient to correct the system's wideband effects. This frequency dependency correction is also apparent when comparing the passband group delay of the measured digitally predistorted signal to that of the measured non-predistorted signal, as seen in Fig. 12.

While the particular amplifier under test had an overall relatively flat group delay response over the given frequency range, there was still a fair amount of variance

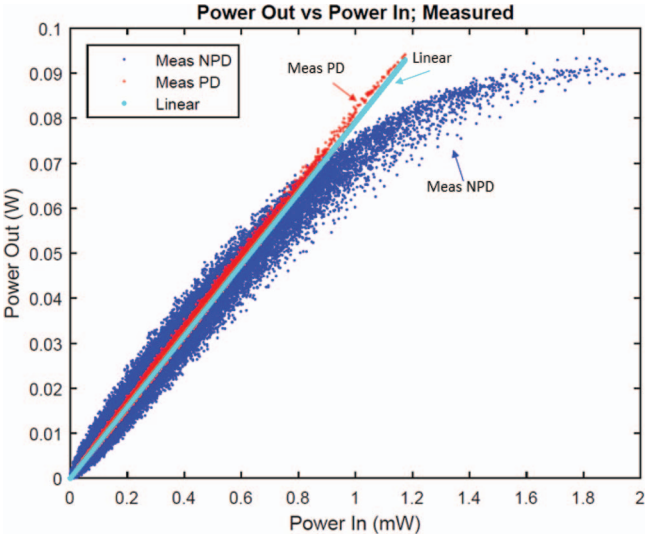

Fig. 11. Power out versus power in of measured predistorted and non-predistorted signals after HPA distortion.

present. The predistorted signal maintained the overall flat group delay response in addition to significantly suppressing the variance throughout the passband, thus significantly improving the accuracy of the overall predistorted system. By producing a linear output power versus input power response, as well as a flat group delay response in the passband, the predistortion approach presented here is shown to be able to accurately reproduce a desired complex baseband waveform. These results, found using a wideband non-constant-modulus waveform with broad instantaneous bandwidth, verify that the DPD approach presented here is not constrained to the traditional constant-modulus class of radar waveforms. This opens the possibility of significantly improved generated signal fidelity and greatly reduced spectral leakage in modern and emerging broadband radar systems

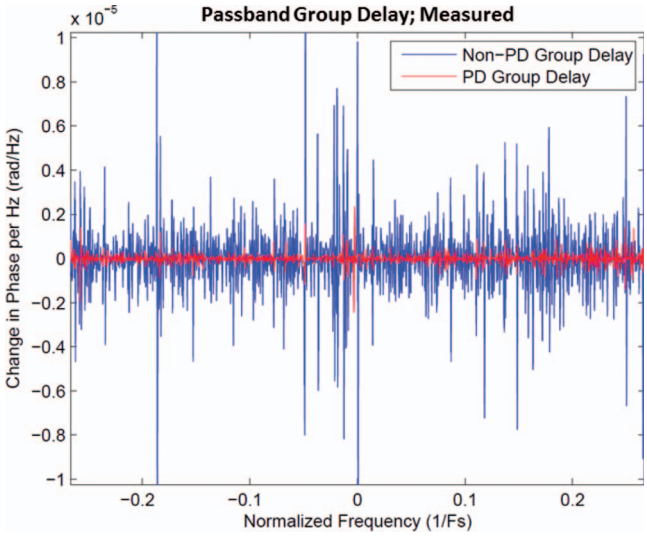

Fig. 12. Passband group delay of measured predistorted and non-predistorted signals after HPA distortion.

that may be dependent upon non-constant-modulus waveforms, such as MIMO radar systems, LPI radars, and SAR systems utilizing wideband beamforming.

IV. CONCLUSION

In conclusion, it has been shown that the Volterra series, and more specifically the MP model, is able to accurately model the nonlinear effects and memory effects of both high-power amplifiers and their associated predistortion models in wideband radar systems. The predistortion model can be implemented digitally in a system and shows potential for significant improvements in radar spectral performance and overall waveform fidelity. These improvements have significant potential impact when used in conjunction with phased array radar architectures utilizing solid-state amplifiers and waveform generators at every antenna element. In the past, least-squares approaches have been shown to be useful to solve DPD model parameters, primarily within the communication community. However, this paper offers a new weighted least-squares approach for wideband radar signals that is more numerically stable. The second technical contribution of this paper is, that for the first time, a Bayesian approach is proposed that allows the models to track slowly changing system parameters to maintain the best current model. Laboratory testing has confirmed the efficacy of this approach. When system data are continuously recorded for system characterization, the Bayesian approach offers long-term computational benefits. DPD allows the radar system to linearly amplify and transmit waveforms over the entire HPA output power range, maximizing power-added efficiency, minimizing spectral spreading, and providing overall performance similar to that of a much larger and more costly radar system that does not utilize DPD. These qualities make DPD a strong contender not only for phased array radar systems, but also for modern radar systems that require high-fidelity generation of eccentric or non-constant-modulus waveforms, such as MIMO radar systems, LPI radars, and SAR systems utilizing wideband beamforming.

REFERENCES

[1] Davis, M.
Frequency allocation challenges for ultra-wideband radars.
IEEE Aerospace and Electronic Systems Magazine, **28**, 7 (Jul. 2013), 12–18.

[2] Nunn, C., and Moyer, L.
Spectrally-compliant waveforms for wideband radar.
IEEE Aerospace and Electronic Systems Magazine, **27**, 8 (Aug. 2012), 11–15.

[3] Yeary, M.
An efficient intermodulation product computing technique for broadband active transmit systems.
IEEE Transactions on Instrumentation and Measurement, **57**, 2 (Feb. 2008), 438–443.

[4] Li, J., and Liu, Q.
PSK communications systems using fully saturated power amplifiers.
IEEE Transactions on Aerospace and Electronic Systems, **42**, 2 (Apr. 2006), 464–477.

[5] Snider, D. M.
A theoretical analysis and experimental confirmation of the optimally loaded and overdriven RF power amplifier.
IEEE Transactions on Electronic Devices, **ED-14**, 12 (Dec. 1967), 851–857.

[6] Benedetto, S., Biglieri, E., and Daffara, R.
Modeling and performance evaluation of nonlinear satellite links—A Volterra series approach.
IEEE Transactions on Aerospace and Electronic Systems, **AES-15**, 4 (Jul. 1979), 494–507.

[7] Javed, A., Goud, P. A., and Syrett, B.
Analysis of a microwave feedforward amplifier using Volterra series representation.
IEEE Transactions on Communications, **25**, 3 (Mar. 1997), 355–360.

[8] Narayanan, S.,
Transistor distortion analysis using Volterra series representation.
The Bell System Technical Journal, **46**, 5 (May–June 1967), 991–1024.

[9] Dunn, Z., Yeary, M., and Fulton, C.
Frequency-dependent power amplifier modeling and correction for distortion in wideband radar transmissions.
In *Proceedings of the IEEE International Midwest Symposium on Circuits and Systems (MWSCAS)*, College Station, TX, Aug. 2014, 1482–1486.

[10] Faulkner, M., and Johansson, M.
Adaptive linearization using predistortion—Experimental results.
IEEE Transactions on Vehicular Technology, **43**, 2 (May 1994), 323–332.

[11] Chappell, W., and Fulton, C.
Digital array radar panel development.
In *Proceedings of the IEEE International Symposium on Phased Array Systems and Technology (ARRAY)*, Waltham, MA, Oct. 2010, 50–60.

[12] Yeary, M., Conway, D., Herd, J., Fosberry, M., Harger, M., and Hondl, K.
A method of improving cross-pol isolation based on the use of auxiliary elements.

In *Proceedings of the IEEE International Symposium on Phased Array Systems and Technology*, Waltham, MA, Oct. 2013.

[13] Zaghloul, A., Kilic, O., and Kohls, E.
System aspects and transmission impairments of active phased arrays for satellite communications.
IEEE Transactions on Aerospace and Electronic Systems, **43**, 1 (Jan. 2007), 176–186.

[14] D'Andrea, A., Lottici, V., and Reggiannini, R.
Efficient digital predistortion in radio relay links with nonlinear power amplifiers.
IEE Proceedings on Communications, **147** (June 2000), 175–179.

[15] Lee, J., Jeon, S., Kim, J., Ryu, H. J., Suh, Y., Mok, H., and Kim, M.
An improved LUT based DPD technique for nonlinear HPA in ATSC DTV system.
In *Proceedings of the IEEE International Symposium on Broadband Multimedia Systems and Broadcasting (BMSB)*, Shanghai, China, March 2010, 1–4.

[16] Han, D., and Hwang, T.
An adaptive pre-distorter for the compensation of HPA nonlinearity.
IEEE Transactions on Broadcasting, **46**, 2 (June 2000), 152–157.

[17] National Telecommunications and Information Administration (NTIA).
Manual of Regulations and Procedures for Federal Radio Frequency Management, Radar Spectrum Engineering Criteria (RSEC). Washington, DC: NTIA, May 2014.

[18] Wicks, M., Mokole, E., Blunt, S., Schneible, R., and Amuso, V.
Principles of Waveform Diversity and Design. Raleigh, NC: SciTech Publishing, Inc., 2010.

[19] Uysal, F., Yeary, M., Goodman, N., Rincon, R., and Osmanoglu, B.
Waveform design for wideband beampattern and beamforming.
In *Proceedings of the IEEE International Radar Conference*, Arlington, VA, May 2015.

[20] Morgan, D., Zhengxiang, M., Jaehyeong, K., Zierdt, M., and Pastalan, J.
A generalized MP model for digital predistortion of RF power amplifiers.
IEEE Transactions on Signal Processing, **54**, 10 (Oct. 2006), 3852–3860.

[21] Kang, H., Cho, Y., and Youn, D.
Adaptive precompensation of Wiener systems.
IEEE Transactions on Signal Processing, **46**, 10 (Oct. 1998), 2825–2829.

[22] Narendra, K., and Gallman, P.
An iterative method for the identification of nonlinear systems using a Hammerstein model.
IEEE Transactions on Automatic Control, **11**, 3 (Jul. 1966), 546–550.

[23] Zhai, J., Zhang, L., Xia, J., Zhou, J., Zhu, X., and Hong, W.
Combined memory polynomial model for Doherty power amplifiers with memory effects.
In *Proceedings of the International Conference on Microwave and Millimeter Wave Technology (ICMMT)*, Vol. 2, Shenzhen, China, May 2012, 1–3.

[24] Ding, L., Zhou, G. T., Morgan, D. R., Ma, Z., Kenney, J. S., Kim, J., and Giardina, C. R.
A robust digital baseband predistorter constructed using memory polynomials.
IEEE Transactions on Communications, **52**, 1 (Jan. 2004), 159–165.

[25] Kim, J., and Konstantinou, K.
Digital predistortion of wideband signals based on power amplifier model with memory.
Electronics Letters, **37**, 23 (Nov. 2001), 1417–1418.

[26] Yu, X., and Jiang, H.
Digital predistortion using adaptive basis functions.
IEEE Transactions on Circuits and Systems I: Regular Papers, **60**, 12 (Dec. 2013), 3317–3327.

[27] Zhu, A., Dooley, J., and Brazil, T.
Simplified Volterra series based behavioral modeling of RF power amplifiers using deviation-reduction.
In *IEEE MTT-S International Microwave Symposium Digest*, San Francisco, CA, June 2006, 1113–1116.

[28] Albert, A.
Regression and the Moore-Penrose Pseudoinverse. New York: Academic Press, 1972.

[29] Courrieu, P.
Fast computation of Moore-Penrose inverse matrices.
Neural Information Processing, **8**, 2 (Aug. 2005), 25–29.

[30] Schetzen, M.
The Volterra and Wiener Theories of Nonlinear Systems. New York: Wiley, 1980.

[31] Raich, R., Qian, H., and Zhou, G. T.
Digital baseband predistortion of nonlinear power amplifiers using orthogonal polynomials.
In *Proceedings of the IEEE International Conference on Acoustics, Speech, and Signal Processing (ICASSP)*, Vol. 6/VI, Hong Kong, China, April 2003, 689–692.

[32] Cline, A., Moler, C., Stewart, G., and Wilkinson, J.
An estimate for the condition number of a matrix.
SIAM Journal on Numerical Analysis, **16** (1979), 368–375.

[33] Vu, V., and Tao, T.
The condition number of a randomly perturbed matrix.
In *Proceedings of the Thirty-Ninth Annual ACM symposium on Theory of Computing*, San Diego, CA, Jun. 2007, 248–255.

[34] Varga, R.
Matrix Iterative Analysis, 2nd ed. New York, NY: Springer., 2000.

[35] Zhai, Y., and Yeary, M.
Implementing particle filters with Metropolis-Hastings algorithms.
In *Proceedings of the IEEE Region 5 Conference*, Oklahoma City, OK, April 2004, 149–152.

[36] Kruschke, J.
Doing Bayesian Data Analysis, A Tutorial with R and BUGS.
Burlington, MA: Academic Press, 2010.

[37] Ristic, B., Farina, A., Benvenuti, D., and Arulampalam, M.
Performance bounds and comparison of nonlinear filters for tracking a ballistic object on re-entry.
IEE Proceedings on Radar, Sonar, and Navigation, **150**, 2 (Apr. 2003), 65–70.

[38] Dunn, Z., Yeary, M., Fulton, C., and Goodman, N.
Wideband solid-state power amplifier modeling and predistortion for radar transmissions.
In *Proceedings of the NATO Science and Technology Organization SET-204 Specialists' Meeting on Waveform Diversity*, Berlin, Germany, September 2014.

[39] Dunn, Z., Yeary, M., Fulton, C., and Goodman, N.
Memory polynomial model for digital predistortion of broadband solid-state radar amplifiers.
In *Proceedings of the IEEE International Radar Conference*, Arlington, VA, May 2015.

[40] Gross, F., and Connor, J.
Comparison of detectability of radar compression waveforms in classic passive receivers.
IEEE Transactions on Aerospace and Electronic Systems, **43**, 2 (Apr. 2007), 789–795.

[41] Qazi, F., and Fam, A.
Doppler detection capable good polyphase code sets based on piecewise linear FM.

In *Proceedings of the IEEE Radar Conference*, Cincinnati, OH, May 2014, 212–217.

[42] Song, X., Zhou, S., and Willett, P.
Enhanced multistatic radar resolution via STC.
IEEE Radar Conference, Pasadena, CA, May 2009, 1–6.

[43] Lewis, B., and Kretschmer, F.
Linear frequency modulation derived polyphase pulse compression codes.
IEEE Transactions on Aerospace and Electronic Systems, **18**, 5 (Sep. 1982), 637–641.

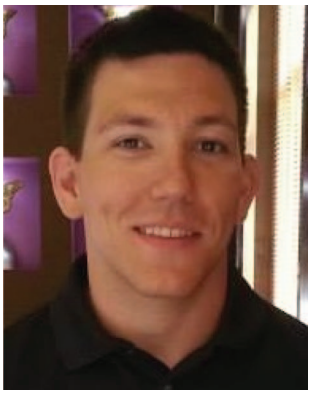

Dr. Zachary Dunn (S'11) received the B.S. degree in engineering physics and Ph.D. degree in electrical and computer engineering from the University of Oklahoma, Norman, OK, in 2011 and 2016, respectively.

He is currently a research assistant with the Advanced Radar Research Center (ARRC), University of Oklahoma. His research interests include radar signal processing, modeling and digital predistortion of solid-state amplifiers, and polarimetric phased array radar systems. He is the recipient of the University of Oklahoma Robert Hughes Centennial Fellowship and 2016 ARRC Student Paper Award. He has spent seven summers interning at NORDAM, Boeing, and Raytheon and joined Raytheon in the Dallas, TX, area as a full-time senior engineer in the summer of 2016.

Dr. Mark Yeary (S'5–M'00–SM'03–F'16) received the B.S. (honors), M.S., and Ph.D. degrees from the Department of Electrical Engineering, Texas A&M University (TAMU), College Station, TX, in 1992, 1994, and 1999, respectively. Since fall 2002, he has been with the School of Electrical & Computer Engineering at the University of Oklahoma (OU), Norman, where he was named the endowed Hudson-Torchmark Presidential Professor in 2011. He is also one of the founding members of the Advanced Radar Research Center (ARRC) at OU.

His research interests are in the areas of digital signal processing (DSP) as applied to customized DSP systems and instrumentation for radar systems with an emphasis on hardware prototype development and practical measurements. He has served as a principal investigator (PI) or co-PI on grants from the National Aeronautics and Space Administration (NASA); National Science Foundation (NSF); National Oceanic & Atmospheric Administration (NOAA); and the Air Force Research Laboratory (AFRL), Raytheon, and Defense Advanced Research Projects Agency (DARPA). Since arriving at OU in 2002, he has supervised and supported 46 undergraduate and graduate students. In addition, he has provided support for eight postdoctoral researchers. He has spent 14 summers (2002–2016) at Raytheon in the Dallas, TX, area, where he is a senior engineer. In the fall of 2012 and spring of 2013, Dr. Yeary joined the Massachusetts Institute of Technology Lincoln Laboratory on sabbatical to make technical contributions related to one of the preliminary radar panels associated with the national Multifunction Phased Array Radar (MPAR) effort.

Dr. Yeary is a fellow of the Institute of Electrical and Electronics Engineers (IEEE), and he is a member of the Tau Beta Pi and Eta Kappa Nu honor societies. In April of 2006, Dr. Yeary received the Outstanding Young Engineer Award from the IEEE. This award was given by the Instrumentation and Measurement Society of the IEEE. This society is devoted to a tight integration of theoretical development, hardware prototyping, and instrumentation design. He is a licensed professional engineer (PE).

Dr. Caleb Fulton (S'05–M'11) received his B.S. and Ph.D. in electrical and computer engineering from Purdue University in West Lafayette, IN, in 2006 and 2011, respectively, and is now an assistant professor in electrical and computer engineering at the University of Oklahoma's Advanced Radar Research Center in Norman, OK. His work focuses on antenna design, digital phased array calibration and compensation for transceiver errors, calibration for high-quality polarimetric radar measurements, integration of low-complexity transceivers and high-power GaN devices, and advanced digital beamforming design considerations. He is currently involved in a number of digital phased array research and development efforts for a variety of applications. He received the Purdue University Eaton Alumni Award for Design Excellence in 2009 for his work on the Army Digital Array Radar (DAR) Project. He also received the Meritorious Paper Award for a summary of these efforts at the 2010 Government Microcircuit Applications and Critical Technologies Conference. More recently, he received a 2015 Defense Advanced Research Projects Agency (DARPA) Young Faculty Award for his ongoing digital phased array research. Dr. Fulton is a member of the Institute of Electrical and Electronics Engineers (IEEE) Antennas and Propagation, Aerospace and Electronic Systems, and Microwave Theory and Techniques Societies, and he serves on the Education Committee of the latter.

Dr. Nathan Goodman (S'98–M'02–SM'07) received the B.S., M.S., and Ph.D. degrees in electrical engineering from the University of Kansas, Lawrence, in 1995, 1997, and 2002, respectively. From 1996 to 1998, he was an radio-frequency systems engineer for Texas Instruments, Dallas, TX. From 1998 to 2002, he was a graduate research assistant in the Radar Systems and Remote Sensing Laboratory, University of Kansas. Dr. Goodman was a faculty member in the Electrical and Computer Engineering Department of the University of Arizona, Tucson, from 2002 to 2011, and is now a professor in the School of Electrical and Computer Engineering and director of research for the Advanced Radar Research Center at the University of Oklahoma, Norman, OK. His research interests are in radar and array signal processing.

Dr. Goodman was awarded the Madison A. and Lila Self Graduate Fellowship from the University of Kansas in 1998. He was also awarded the Institute of Electrical and Electronics Engineers (IEEE) 2001 International Geoscience and Remote Sensing Symposium Interactive Session Prize Paper Award. Dr. Goodman has served as technical cochair for the 2011 IEEE Radar Conference, finance chair for the IEEE Sensor Array and Multichannel Signal Processing Workshop (SAM 2012), associate editor-in-chief for Elsevier's *Digital Signal Processing* journal. He is currently an associate editor for *IEEE Transactions on Aerospace and Electronic Systems* and is serving as cochair for the North Atlantic Treaty Organization (NATO) SET-227 Research Task Group on Cognitive Radar. Dr. Goodman is a senior member of the IEEE.